Supporting Information

Polypyrrole Nanotunnels with Luminal and Abluminal Layered Double Hydroxide Nanosheets Grown on a Carbon Cloth for Energy Storage Applications

Prakash Chandra Lohani [a, b], Arjun Prasad Tiwari [a], Kisan Chhetri [a], Alagan Muthurasu [a], Bipeen Dahal [a], Su-Hyeong Chae [a], Tae Hoon Ko [a], Jun Youb Lee [c], Yong Sik Chung [d], Hak Yong Kim [a, d*]

[a]Department of Nano Convergence Engineering, Jeonbuk National University, Jeonju 561-756, Republic of Korea

[b]Department of Chemistry, Amrit Campus, Tribhuvan University, Kathmandu 44613, Nepal

[c]O-Sung Co. Ltd, Jeonju 54853, Republic of Korea

[d]Department of Organic Material and Fiber Engineering, Jeonbuk National University, Jeonju 561-756, Republic of Korea

[*]Corresponding Author: E-mail; khy@jbnu.ac.kr (Prof. Hak Yong Kim)

Tel.: +82 63 273 2351: Fax: +82 63 270 4249

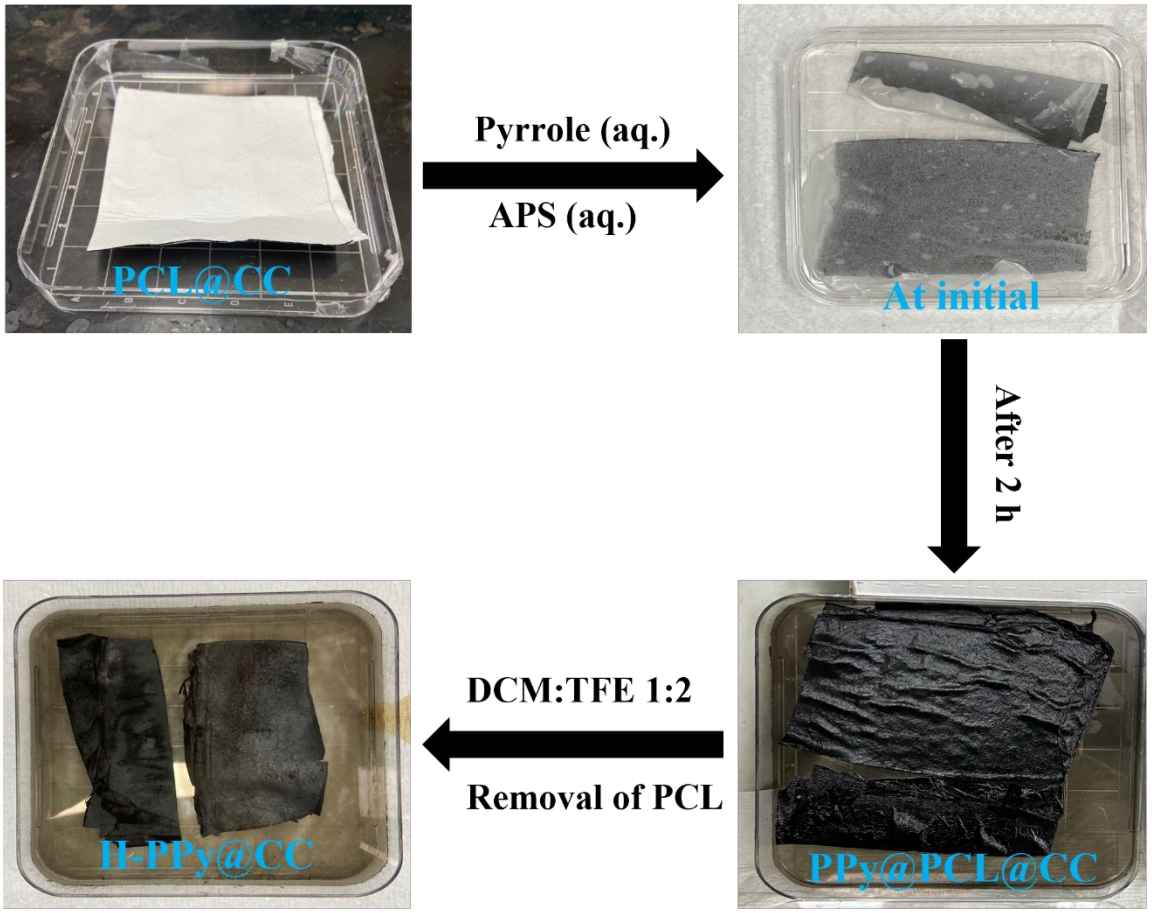

Figure S1. Digital photographs for the fabrication of H-PPy@CC.

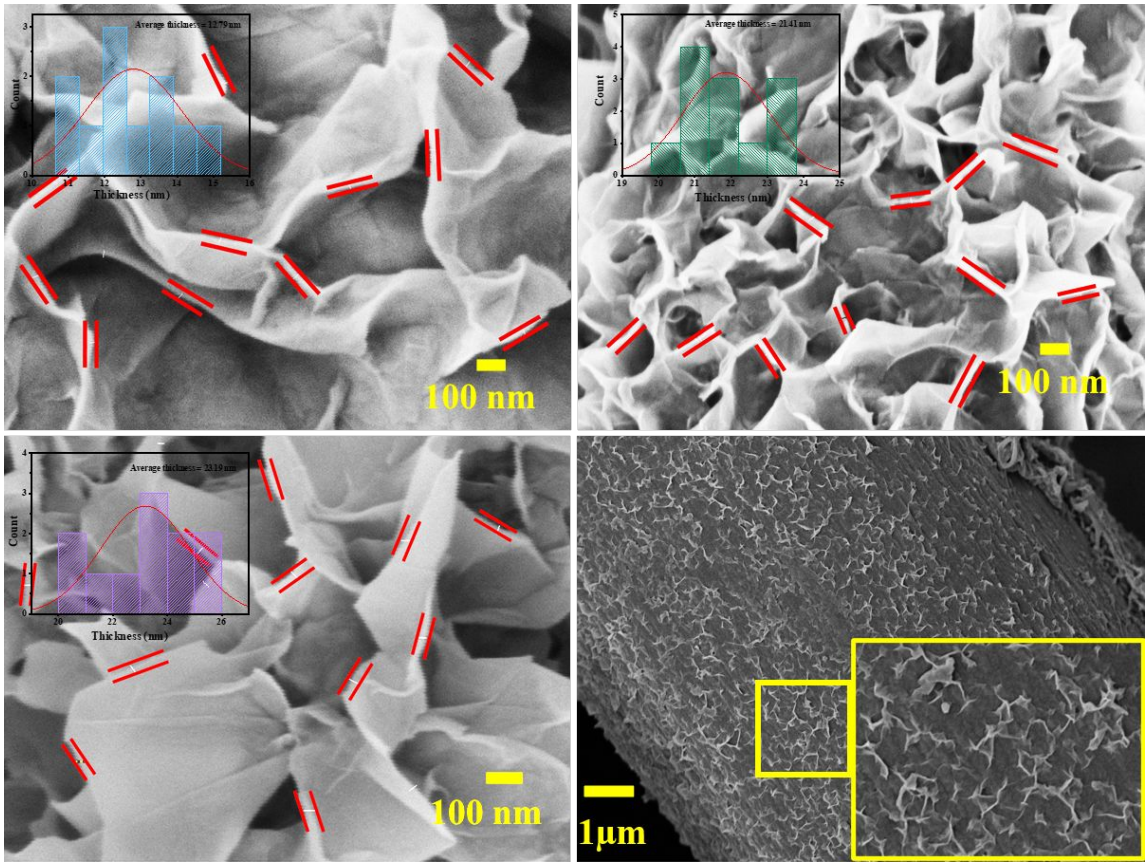

Figure S2. FESEM images of (A) NiCo-LDH@H-PPy@CC (1:1), (B) NiCo-LDH@H-PPy@CC (2:1), (C) NiCo-LDH@H-PPy@CC (1:2), and (D) NiCo-LDH@CC (insets in Figs. A, B and C represent histograms displaying the average thickness of the NiCo-LDH nanosheets).

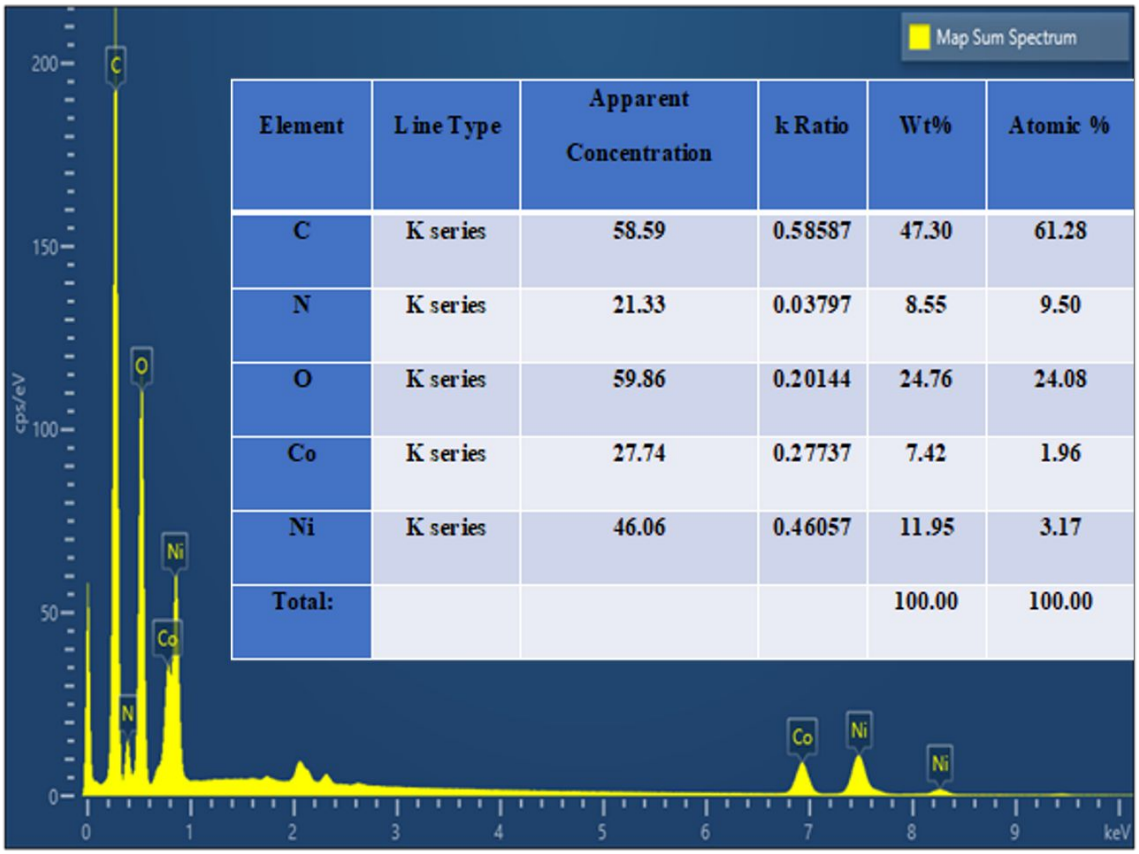

Element	Line Type	Apparent Concentration	k Ratio	Wt%	Atomic %
C	K series	58.59	0.58587	47.30	61.28
N	K series	21.33	0.03797	8.55	9.50
O	K series	59.86	0.20144	24.76	24.08
Co	K series	27.74	0.27737	7.42	1.96
Ni	K series	46.06	0.46057	11.95	3.17
Total:				100.00	100.00

Figure S3. EDS spectrum for NiCo-LDH@H-PPy@CC (inset shows the percentage of elements constituting NiCo-LDH@H-PPy@CC).

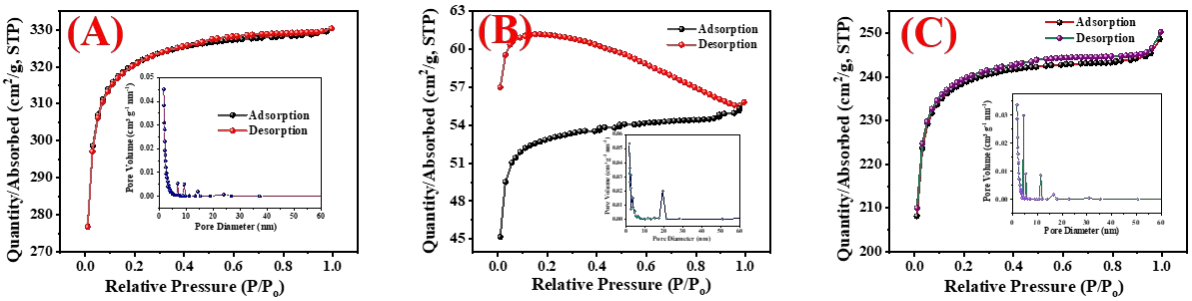

Figure S4. BET analysis of (A) pure CC, (B) PPy@PCl@CC, and (C) H-PPy@CC.

Table S1. BET data for various materials.

S. N	Materials	BET surface area (m^2 g^{-1})	BJH Adsorption cumulative volume of pore (cm^3 g^{-1})	BJH Adsorption Average pore diameter [nm]
1	Carbon Cloth (CC)	1269.2907	0.038948	2.6581
2	PPy-PCL@CC	210.3801	0.008305	3.5663
3	H-PPy@CC	944.8180	0.034902	3.41864
4	NiCo-LDH@H-PPy@CC(1:1)	728.9379	0.039080	4.1183

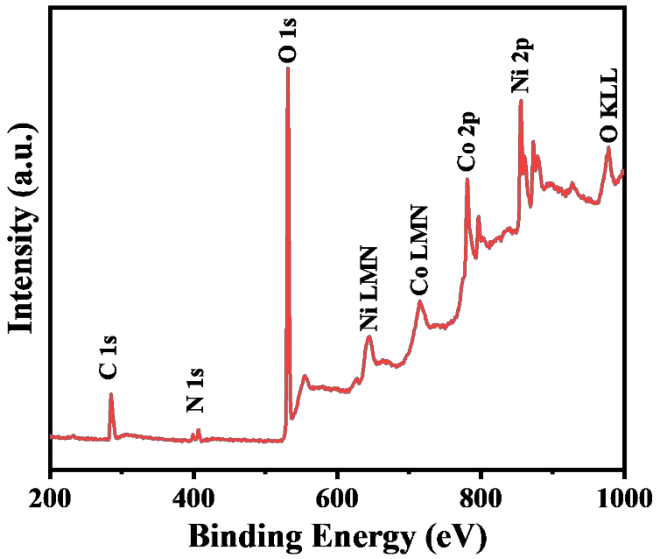

Figure S5. XPS full spectra for NiCo-LDH@H-PPy@CC(1:1).

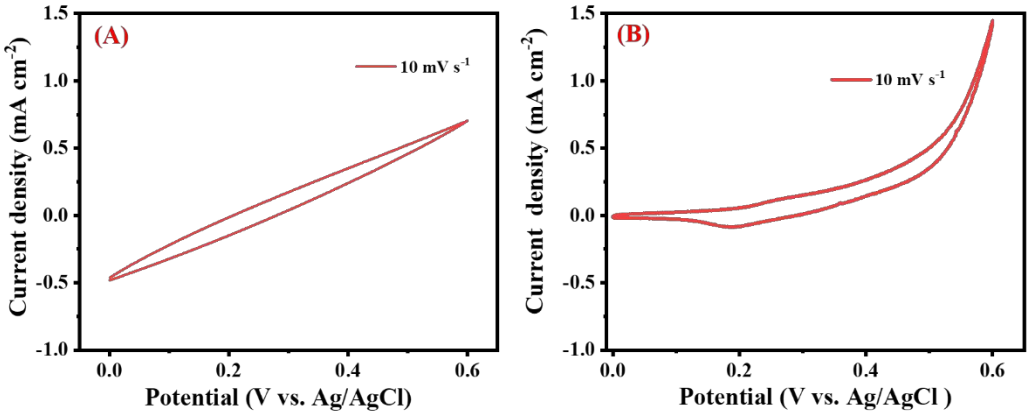

Figure S6. CV curves for (A) pure CC and (B) H-PPy@CC.

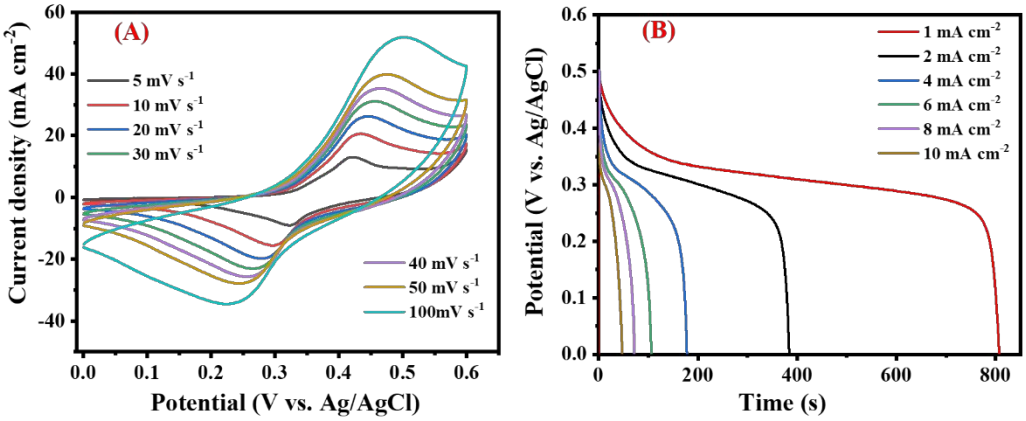

Figure S7. (A) CV and (B) GCD profiles for NiCo-LDH@H-PPy@CC (2:1).

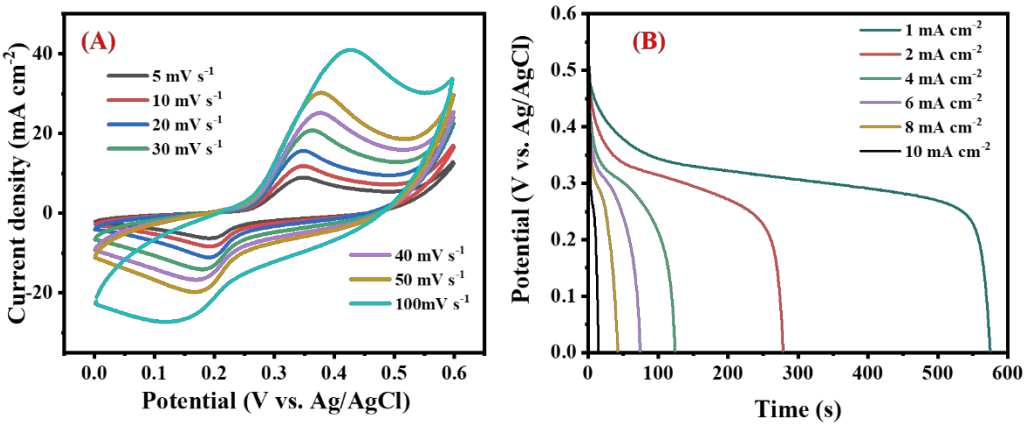

Figure S8. (A) CV and (B) GCD profiles for NiCo-LDH@H-PPy@CC (1:2).

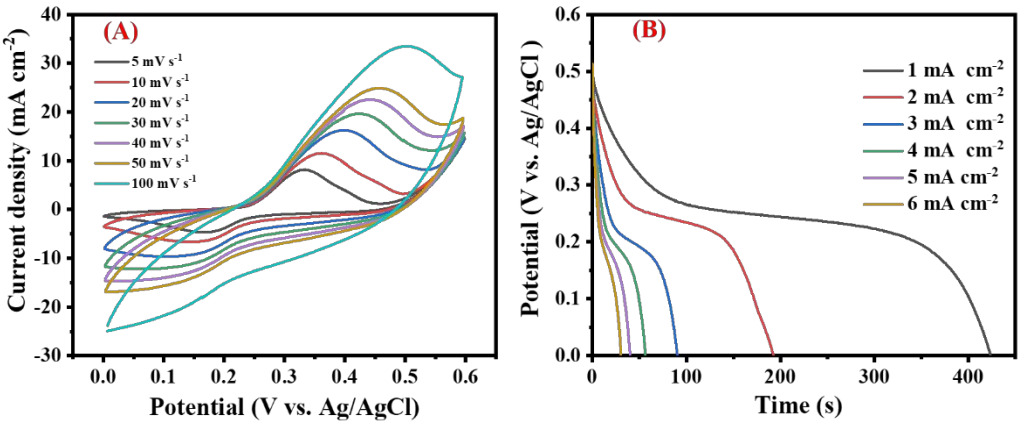

Figure S9. (A) CV and (B) GCD profiles for NiCo-LDH@H-PPy@CC (SS).

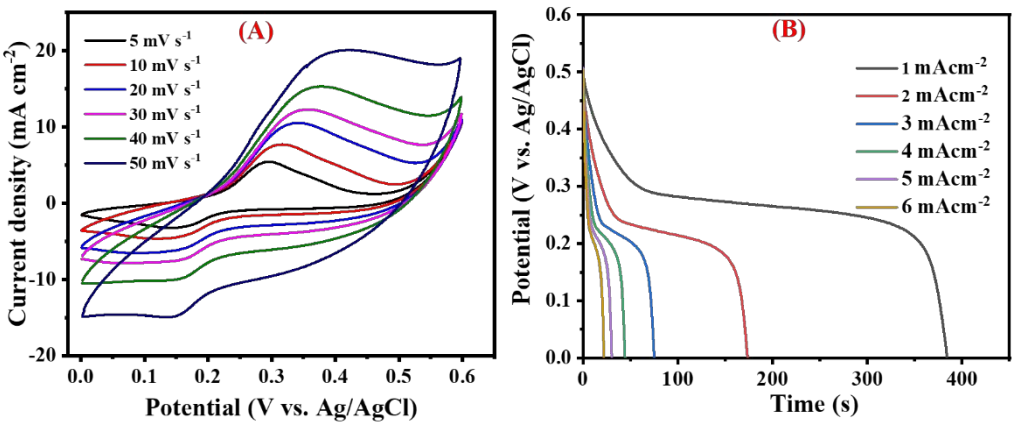

Figure S10. (A) CV and (B) GCD profiles for NiCo-LDH@PPy@PCl@CC.

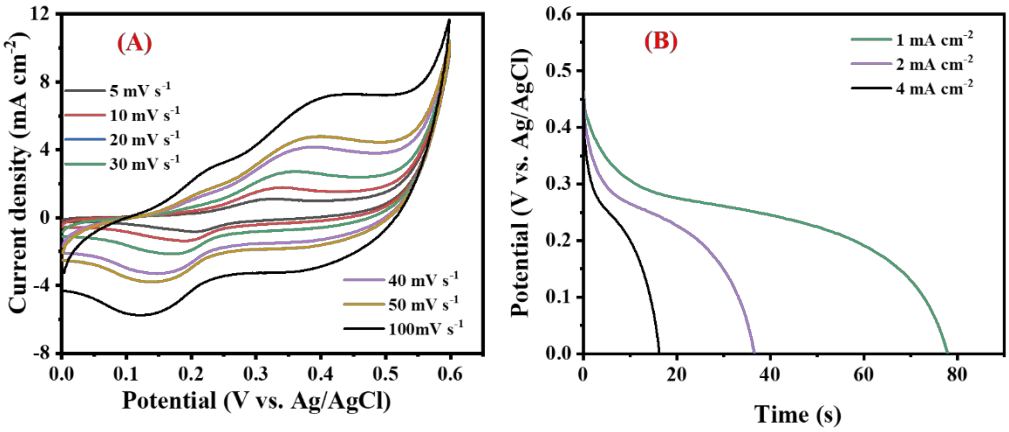

Figure S11. (A) CV and (B) GCD profiles for NiCo-LDH@CC.

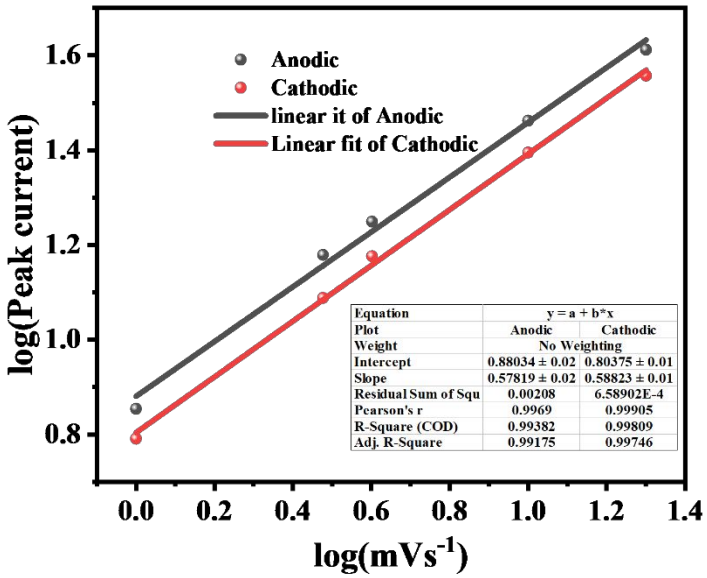

Equation	y = a + b*x	
Plot	Anodic	Cathodic
Weight	No Weighting	
Intercept	0.88034 ± 0.02	0.80375 ± 0.01
Slope	0.57819 ± 0.02	0.58823 ± 0.01
Residual Sum of Squ	0.00208	6.58902E-4
Pearson's r	0.9969	0.99905
R-Square (COD)	0.99382	0.99809
Adj. R-Square	0.99175	0.99746

Figure S12. Logarithm of the peak current [log(i)] versus the logarithm of the scan rate [log((V)) for NiCo-LDH@H-PPy@CC

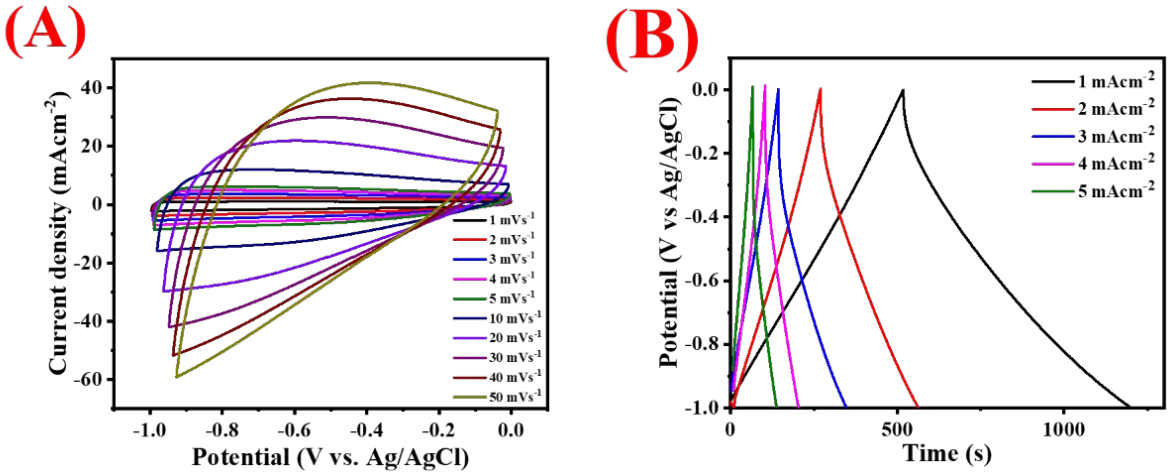

Figure S13. CV (A) and GCD (B) profiles for the negative electrode material (VPO@CNFs900)

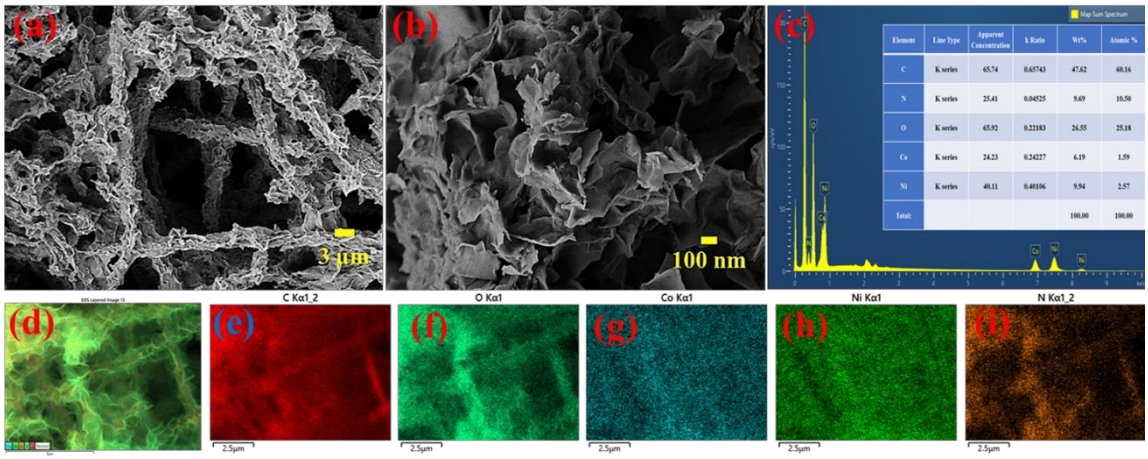

Figure S14. FESEM images of (a, b), (c) EDX and (d-i) elemental mapping for NiCo-LDH@H-PPy@CC (1:1) after stability testing.

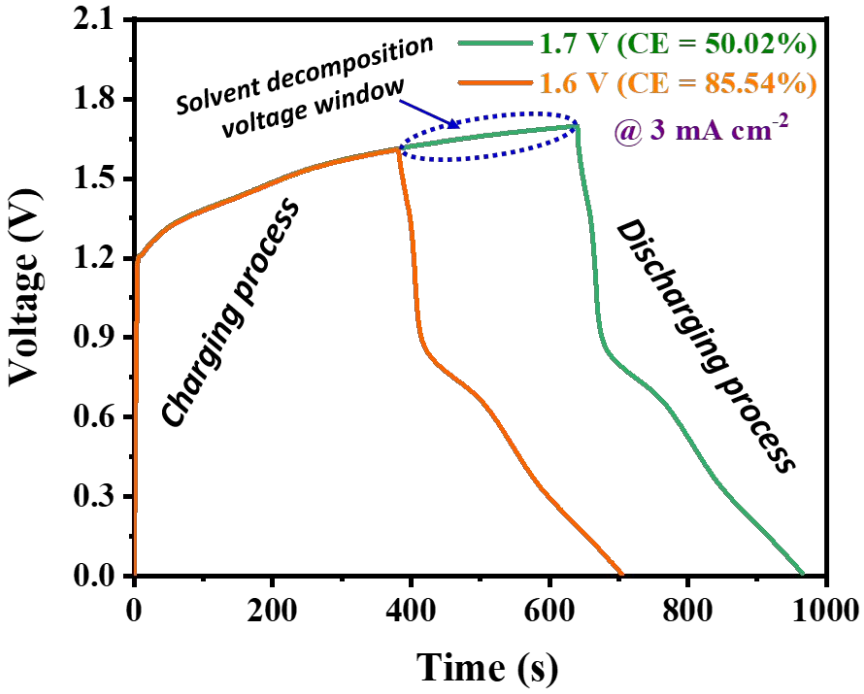

Figure S15. Charging and discharging behavior of ASC device at 6 mA cm^{-2} under the different potential windows

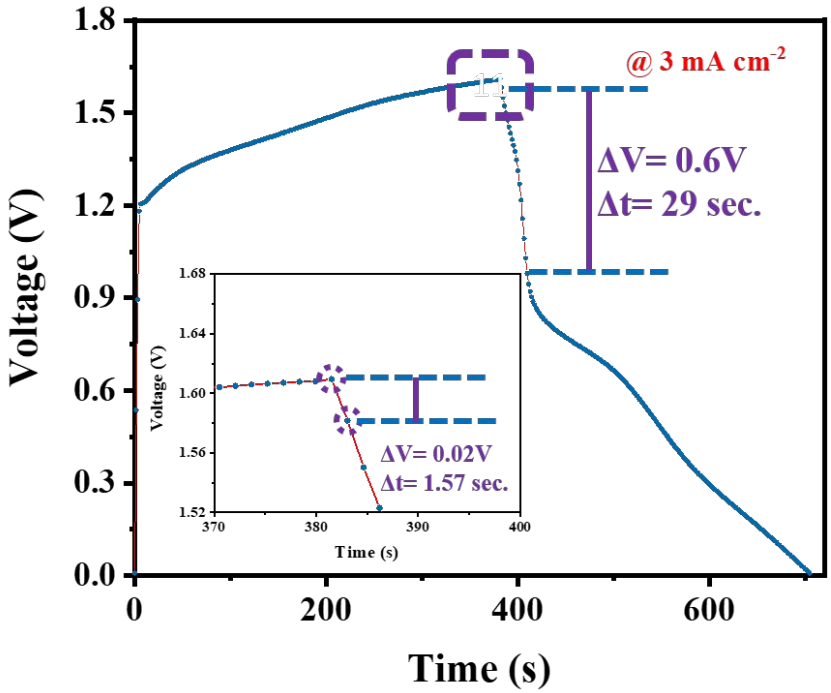

Figure S16. GCD cruve of ASC device at 3 mA cm^{-2} under working potential of 1.6 V.

Table S2. Comparison of the capacity, stability and rate capability values obtained for the different electrode materials studied in this work

Electrode materials	Current density (A g^{-1})	Specific capacity (mAh g^{-1})	Rate capability @ 6mAh g^{-1} (%)	Capacitance retention (%)
NiCo-LDH@H-PPy@CC (1;1)	1	149.16		93.4
	2	141.5		
	4	138.6		
	6	133.33	89.4	
	8	126.2		
	10	121.66		
	12	120		
NiCo-LDH@H-PPy@CC (2:1)	1	139.7		
	2	128.8		
	4	111.11		
	6	93.33	66.80	
	8	84.22		
	10	70.17		
NiCo-LDH@H-PPy@CC (1:2)	1	98		
	2	90.86		
	4	74.6		
	6	64.5	65.8	

	8	**45.15**		
	10	**19.11**		
NiCo-LDH@H-PPy@CC(SS)	**1**	**80**		
	2	**70**		
	3	**56**		
	4	**40**		
	5	**33**		
	6	**26.6**	**33.33**	
NiCo-LDH @PPy@PCL@CC	**1**	**67**		
	2	**57**		
	3	**41**		
	4	**30**		
	5	**24**		
	6	**18**	**26.86**	
NiCo-LDH @CC	**1**	**26.1**		
	2	**20.33**		
	4	**11.11**		

Table S3. Comparison of the specific capacity/capacitance with that previously reported in the literature.

S.N.	Electrode materials	Specific capacitance/ capacity	Electrolyte used	Rate capability (A g^{-1})	Ref.
1	**NiCo-LDH @H-PPy@CC**	**149.16 mA h g^{-1} at 1 mA cm^{-2} (1098 F g^{-1} at 1 A g^{-1})**	**2 M KOH**	**85.25% (1-12) 1 mA cm^{-2}**	**This work**
2	NiCo LDH	1537 F g^{-1} (0.5 A g^{-1})	6 M KOH	77% (1-10) A g^{-1}	1
3	NiCo LDH/NCF	855.4 F g^{-1} (1 A g^{-1})	6 M KOH	91% (1-10) A g^{-1}	2
4	NiCo LDH/AC	947 F g^{-1} (1 A g^{-1})	6 M KOH	63% (1-20) A g^{-1}	3
5	PANI/NiCo-LDH	1845 Fg^{-1} (0.5 A g^{-1})	2 M KOH	82.1% (1-10) A g^{-1}	4
6	PANC@Co–Ni LDH	1529.52 F g^{-1} (0.5 A g^{-1})	6 M KOH	94.3% (1-10) A g^{-1}	5
7	NiCo binary hydroxide (1:1)	804 F g^{-1} (3 A g^{-1})	6 M KOH	-	6
8	$Ni(OH)_2$/PNTs	864 F g^{-1} (1 A g^{-1})	6 M KOH	73.4% (1-8) A g^{-1}	7
9	CoAl-LDH/PPy/Graphene	864 F g^{-1} (1 A g^{-1})	30 wt % KOH	75% (1-20) A g^{-1}	8
10	CoAl-LDH/PEDOT/Nickel foil	672 F g^{-1} (1 A g^{-1})	6 M KOH	63% (1-40) A g^{-1}	9

11	NiAl-LDH/PPy/Graphene	845 F g^{-1} 2 mVs^{-1}	1 M KOH	67% (1-30) A g^{-1}	10

Table S4. Specific rate capacity, current density and power density of the ASC device (NiCo-LDH@H-PPy@CC//VPO@CNFs900) at different current densities.

SN	Current Density (mA cm^{-2})	specific rate capacity (mAh g-1)	Specific Energy Density (Wh kg^{-1})	Specific Power Density (W kg^{-1})
1	**3**	**40.53**	**32.42**	**359.16**
2	**4**	**36.7**	**29.36**	**477.46**
3	**5**	**33.8**	**27.04**	**596.18**
4	**6**	**30.7**	**24.56**	**722.03**
5	**10**	**26.5**	**21.2**	**1215.31**
6	**14**	**25.78**	**20.62**	**1630.72**
7	**18**	**25.08**	**20.06**	**1999.89**

Table S5. Summary of some recently published work for NiCo-LDH based ASC devices.

S.N.	ASC Device	Device Window (V)	Energy Density (Wh kg ^{1})	Power Density (W kg ^{1})	Cyclic stability	Ref.
1	NiCo-LDH@Ni-CAT//AC	0-1.6	23.5	394.6	82% After 10,000 Cycles	[11]
2	NiCo-LDH	0-1.5	26.3	320	110% after 700 cycles at 100 mVs^{-1}	[6]
3	4 M-P@NiCo-LDH//AC	0-1.5	18.1	750	77.17% after 5000 cycles at 10 A g^{-1}	[12]
4	NiCo LDH @ Zn_2SnO_4//AC	0-1.2	23.7	284.2	92.7% 5000 cycles at 50 mVs^{-1}	[13]
5	Ni-Co LDH/GNR//AC	0-1.5	25.4	749	96% after 5000 cycles at	[14]

					2 A g^{-1}	
6	$NiCo_2O_4$-RGO//AC	0-1.4	23.3	324.9	93% after 2500 cycles at 2 A g^{-1}	[15]
7	CoMn LDH/PPy//MLG	0-1.5	29.6	0.5	99.5% after 8000 cycles at 5 A g^{-1}	[16]
8	LDH/PC-1//AC	0-1.5	18.60	225.03	84.58% after 3000 at 15 A g^{-1}	[17]
9	Ni-Co-Zn hydroxide//AC	0-1.5	16.62	2900	84% after 1000 cycles at 2 A g^{-1}	[18]
10	Ni-Co Oxide//AC	0-1.3	12	95.2	85% after 2000 cycles at 8 A g^{-1}	[19]
11	**NiCo-LDH @H-PPy@CC**//VPO@CNFs900	**0-1.6**	**32.42**	**359.16**	**94.09% after 10000 cycles (10 mA cm^{-2})**	**This Work**

References

1. Li, R.; Hu, Z.; Shao, X.; Cheng, P.; Li, S.; Yu, W.; Lin, W.; Yuan, D., Large Scale Synthesis of NiCo Layered Double Hydroxides for Superior Asymmetric Electrochemical Capacitor. *Scientific Reports* **2016,** *6* (1), 18737.

2. Meng, X.; Feng, M.; Zhang, H.; Ma, Z.; Zhang, C., Solvothermal synthesis of cobalt/nickel layered double hydroxides for energy storage devices. *Journal of Alloys and Compounds* **2017,** *695*, 3522-3529.

3. Chen, T.; Luo, L.; Wu, X.; Zhou, Y.; Yan, W.; Fan, M.; Zhao, W., Three dimensional hierarchical porous nickel cobalt layered double hydroxides (LDHs) and nitrogen doped activated biocarbon composites for high-performance asymmetric supercapacitor. *Journal of Alloys and Compounds* **2021,** *859*, 158318.

4. Ge, X.; He, Y.; Plachy, T.; Kazantseva, N.; Saha, P.; Cheng, Q., Hierarchical PANI/NiCo-LDH Core-Shell Composite Networks on Carbon Cloth for High Performance Asymmetric Supercapacitor. *Nanomaterials* **2019,** *9* (4).

5. Cao, J.; Li, L.; Xi, Y.; Li, J.; Pan, X.; Chen, D.; Han, W., Core–shell structural PANI-derived carbon@Co–Ni LDH electrode for high-performance asymmetric supercapacitors. *Sustainable Energy & Fuels* **2018,** *2* (6), 1350-1355.

6. Sun, X.; Wang, G.; Sun, H.; Lu, F.; Yu, M.; Lian, J., Morphology controlled high performance supercapacitor behaviour of the Ni–Co binary hydroxide system. *Journal of Power Sources* **2013,** *238*, 150-156.

7. Zhang, J.; Liu, Y.; Guan, H.; Zhao, Y.; Zhang, B., Decoration of nickel hydroxide nanoparticles onto polypyrrole nanotubes with enhanced electrochemical

performance for supercapacitors. *Journal of Alloys and Compounds* **2017,** *721*, 731-740.

8. Zhang, Y.; Du, D.; Li, X.; Sun, H.; Li, L.; Bai, P.; Xing, W.; Xue, Q.; Yan, Z., Electrostatic Self-Assembly of Sandwich-Like CoAl-LDH/Polypyrrole/Graphene Nanocomposites with Enhanced Capacitive Performance. *ACS Applied Materials & Interfaces* **2017,** *9* (37), 31699-31709.

9. Han, J.; Dou, Y.; Zhao, J.; Wei, M.; Evans, D. G.; Duan, X., Flexible CoAl LDH@PEDOT Core/Shell Nanoplatelet Array for High-Performance Energy Storage. *Small* **2013,** *9* (1), 98-106.

10. Li, X.; Zhang, Y.; Xing, W.; Li, L.; Xue, Q.; Yan, Z., Sandwich-like graphene/polypyrrole/layered double hydroxide nanowires for high-performance supercapacitors. *Journal of Power Sources* **2016,** *331*, 67-75.

11. Li, Y.; Li, Q.; Zhao, S.; Chen, C.; Zhou, J.; Tao, K.; Han, L., Conductive 2D Metal-Organic Frameworks Decorated on Layered Double Hydroxides Nanoflower Surface for High-Performance Supercapacitor. *ChemistrySelect* **2018,** *3* (48), 13596-13602.

12. Wang, G.; Jin, Z.; Zhang, W., A phosphatized NiCo LDH 1D dendritic electrode for high energy asymmetric supercapacitors. *Dalton Transactions* **2019,** *48* (39), 14853-14863.

13. Wang, X.; Sumboja, A.; Lin, M.; Yan, J.; Lee, P. S., Enhancing electrochemical reaction sites in nickel–cobalt layered double hydroxides on zinc tin oxide nanowires: a hybrid material for an asymmetric supercapacitor device. *Nanoscale* **2012,** *4* (22), 7266-7272.

14. Jin, H.; Yuan, D.; Zhu, S.; Zhu, X.; Zhu, J., Ni–Co layered double hydroxide on carbon nanorods and graphene nanoribbons derived from MOFs for

supercapacitors. *Dalton Transactions* **2018,** *47* (26), 8706-8715.

15. Wang, X.; Liu, W. S.; Lu, X.; Lee, P. S., Dodecyl sulfate-induced fast faradic process in nickel cobalt oxide–reduced graphite oxide composite material and its application for asymmetric supercapacitor device. *Journal of Materials Chemistry* **2012,** *22* (43), 23114-23119.

16. Guo, Y.; Zhang, S.; Wang, J.; Liu, Z.; Liu, Y., Facile preparation of high-performance cobalt–manganese layered double hydroxide/polypyrrole composite for battery-type asymmetric supercapacitors. *Journal of Alloys and Compounds* **2020,** *832*, 154899.

17. Yu, M.; Liu, R.; Liu, J.; Li, S.; Ma, Y., Polyhedral-Like NiMn-Layered Double Hydroxide/Porous Carbon as Electrode for Enhanced Electrochemical Performance Supercapacitors. *Small* **2017,** *13* (44), 1702616.

18. Wang, H.; Gao, Q.; Hu, J., Asymmetric capacitor based on superior porous Ni–Zn–Co oxide/hydroxide and carbon electrodes. *Journal of Power Sources* **2010,** *195* (9), 3017-3024.

19. Tang, C.; Tang, Z.; Gong, H., Hierarchically Porous Ni-Co Oxide for High Reversibility Asymmetric Full-Cell Supercapacitors. *Journal of The Electrochemical Society* **2012,** *159* (5), A651-A656.